Conductivity relaxation in the interfacial phase of iron core–iron oxide shell nanocomposites

S. Basu[a)]
Unit on Nano Science and Technology, Indian Association for the Cultivation of Science,
Kolkata–700032, India

J.R. Macdonald
Department of Physics and Astronomy, University of North Carolina,
Chapel Hill, North Carolina 27599-3255

D. Chakravorty
Unit on Nano Science and Technology, Indian Association for the Cultivation of Science,
Kolkata–700032, India

The alternating current electrical conductivity of a gel-derived glass of composition $55Fe_2O_3 \cdot 45SiO_2$ (mol%) was measured over a frequency range of 100 Hz to 6 MHz. The gel was subjected to a reduction treatment at 923 K for ½ h and subsequently heated in ordinary atmosphere at a temperature 773 K for ½ h to grow a Fe-core Fe_3O_4 shell nanostructure with a median diameter of 6.2 nm. This formed a percolative network within the silica gel. Mossbauer spectra confirmed the presence of Fe_3O_4 in the nanoshell. Electrical measurements were also carried out on these nanocomposites at different frequencies and temperatures. Isothermal electrical modulus data for both reference and treated glass systems were analyzed using both the CK0 and CK1 Kohlrausch-related frequency response models. Reference-glass shape parameter values, estimated by fitting the experimental data to the K0 model at several temperatures, were found to be ~0.32. Here, the K0 model led to much better fits than the K1 did. However, for the treated core–shell-structured nanocomposite material, both models yielded good fits with consistent but different shape parameter estimates: very close to ½ for the K0 model and ⅓ for the K1 model. In accordance with the structural measurements and with axiomatic topological considerations that predict a shape-parameter value of ⅓ for one-dimensional motion and ½ for two-dimensional motion, it appears that the ~0.32 value is consistent with one-dimensional motion of charge carriers along the narrow channels of the interconnected iron-rich three-dimensional phase of the reference glass. Further, although the K1-model ⅓ estimates for the treated material also indicate the presence of one-dimensional charge motion at the two-dimensional interface between the two interconnected phases of the reference glass, the ½ K0 estimates for the same material suggest an effective charge-motion dimension of 2. Importantly, comparison of the high-frequency dielectric constant estimates for the K0 reference glass and the K1 treated one clearly leads to the new but physically plausible conclusion that the bulk frequency-independent dielectric constant of about 30 is independent of the treatment.

I. INTRODUCTION

Physical properties of nanostructured materials have received much attention in recent years.[1–6] Nanocrystalline materials are characterized by a large number of interfaces. The structure and properties of silicon thin films were, in fact, analyzed on the basis of a confined amorphous equilibrium phase.[7] Surface-controlled structure transformation in nanoparticles has also been reported.[8] In some recent experiments, we have grown composites of Fe–Fe_3O_4 core–shell nanostructure within a silica gel, the nanophase having a percolative configuration.[9] The electrical conductivity was found to be drastically different from that of the precursor gel. The property was ascribed to an interfacial phase. Conductivity dispersion as a function of frequency has been used to

study the structure of various glass systems and their conduction mechanisms.[10–12]

Recently, we applied a new data analysis method[13–15] to study the system composed of copper-core copper-oxide shell nanocomposites.[16] Two Kohlrausch-related frequency response models were used to analyze the complex electrical conductivity data for the interfacial amorphous phase in this system. The analysis was carried out for both the precursor reference glass and for the glass containing the core–shell nanostructure. Complex nonlinear-least-squares data fitting showed that the shape parameter β_1 was consistent with the values ⅓ and ⅔ for the reference glass and the nanocomposite glass, respectively. In the present paper, we report results of an investigation of nanocomposites containing $Fe–Fe_3O_4$ core–shell structures grown within a silica gel matrix. To shed some light on the structure of the interfacial phase we have not only studied the Mossbauer spectra of these materials but have also analyzed their frequency response behavior in detail, as discussed herein.

II. EXPERIMENTAL DETAILS

The composition of the gel used in our work was $55Fe_2O_3 \cdot 45SiO_2$ (mol%).

$FeCl_3$ and tetraethylorthosilicate were taken as precursors; 23.174 g $FeCl_3$ was mixed with 60 ml ethyl alcohol and 10 ml distilled water. The solution was stirred for 20 min. A second solution was prepared by adding 26.2 ml tetraethylorthosilicate to 90 ml ethyl alcohol, 15 ml distilled water, and 1 ml HCl. After stirring for 1 h, the two solutions were mixed and stirring continued for another hour. The solution thus prepared was allowed to gel for two weeks. The gel was then reduced in hydrogen at 923 K for ½ h. The gel powder was packed in a graphite mold with a diameter of 1 cm and then hot pressed at 923 K for 5 min in a sintering press DSP 25ATS, supplied by Dr. Fritsch Sondermaschinen GmbH (Stuttgart, Germany). The mold chamber was evacuated to a pressure of $\sim 7.0 \times 10^{-3}$ Torr, and the pressure applied was 2.4 MPa.

The resulting sample showed metallic conduction, indicating that the iron particles formed a percolative network. This was, however, not true for the reference glass, as discussed below. Electron microscopic investigation (described later) showed the average diameter of iron particles to be 5.3 nm. The reduced gel powders were subjected to heat treatment in ordinary atmosphere at temperatures in the range 573–973 K for ½ h. This produced an oxide layer on the nanoparticles of iron. These powders were then hot pressed following the procedure described above. The resulting sample constituted the core–shell nanocomposite.

The reference sample was prepared by first heating gel powder at 1123 K for 2 h at ordinary atmosphere and then hot pressed. Microstructural studies were carried out using a JEM 2010 transmission electron microscope (Tokyo, Japan). Specimen preparation details have been described earlier.[17] For electrical measurements, the specimen faces were vacuum-coated with gold electrodes. The impedance was measured over the frequency range 100 Hz to 6 MHz using a Hewlett Packard HP 4192A impedance analyzer (Tokyo, Japan). Measurements were carried out over the temperature range of 120–440 K.

Mossbauer spectra of the nanocomposites were recorded in a conventional spectrometer operating in constant acceleration mode having 1024 channels. The spectrometer was calibrated with a pure natural iron foil of 15 μm thickness. A 10 m Ci $^{57}C_0$ in Rh matrix was used as the radioactive source. The spectra were fitted to Lorentzian lineshapes by least-squares.

III. STRUCTURAL RESULTS

Figure 1 is a transmission electron micrograph for the reference sample. It is seen that the microstructure consists of two interconnected phases, the darker one indicating the iron-rich phase. The latter has a width of ~5.5 nm. Figure 2(a) shows the electron micrograph for the specimen reduced in hydrogen at 923K for ½ h and then heat treated at 773K for ½ h. Figure 2(b) is the electron diffraction pattern taken on the particles seen in Fig. 2(a).

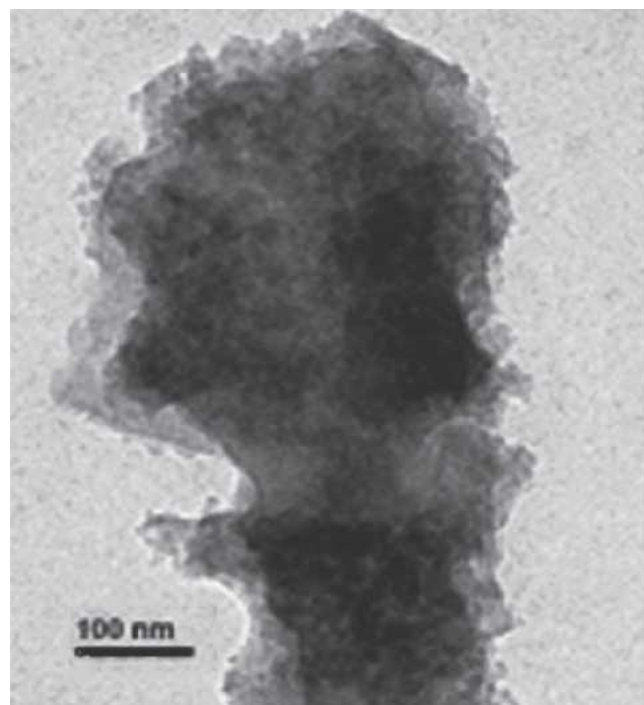The interplanar spacings were calculated from the angle of diffraction determined from the spots. The

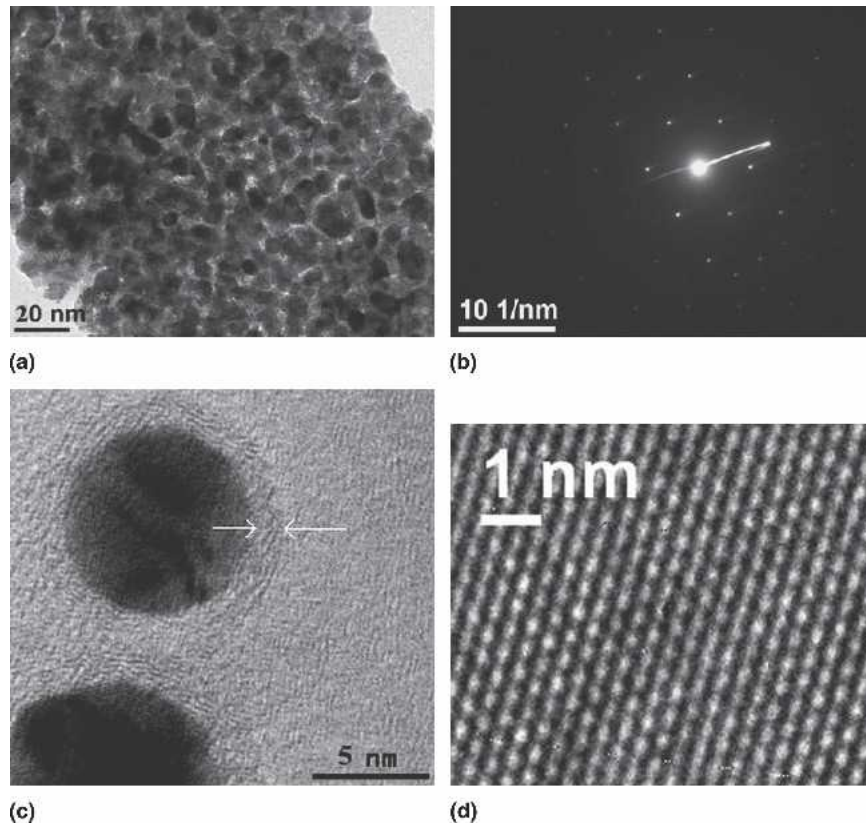FIG. 1. Transmission electron micrograph for the reference glass sample.

FIG. 2. (a) Transmission electron micrograph for specimen reduced at 923 K for ½ h followed by heat treatment at 773 K for ½ h. (b) Electron diffraction pattern from particles seen in (a). (c) Transmission electron micrograph of Fe core–Fe_3O_4 shell structure. (d) High-resolution lattice image of a Fe core–Fe_3O_4 shell nanocomposite.

d_{hkl} values are given in Table I. The results indicate the presence of Fe and Fe_3O_4 phases in the particles having core-shell structures. Figure 2(c) is a typical micrograph of a core of Fe of diameter 7.5 nm and shell of Fe_3O_4 of thickness 1.2 nm. In Fig. 2(d), we show the high resolution lattice images of the core–shell structure. Three sets of planes are seen. The lattice spacing of these planes are measured as 0.26 nm [Fe_3O_4 ($\bar{1}02$)], 0.23 nm [Fe_3O_4 ($\bar{1}12$)], and 0.19 nm [Fe_3O_4 ($\bar{2}10$) and Fe (110)]. These confirm the presence of Fe and Fe_3O_4 in the composite particles. Figure 3 gives the histogram of composite particles. The points represent the experimental

TABLE I. Interplanar spacings d_{hkl} obtained from electron diffraction pattern of nano-core–shell composite particles. The Miller indices of planes are shown within parentheses.

d_{hkl} observed (nm)	d_{hkl}, ASTM (nm)	
	α–Fe	Fe_3O_4
0.202	0.2026(110)	
0.178		0.1712(422)
0.112		0.1121(642)
0.109		0.1092(731)
0.100	0.1013(220)	
0.096		0.0969(751)
0.090	0.0906(222)	

data, and the line is the theoretically fitted log-normal distribution function. The median diameter and the geometric standard deviation extracted from this fitting are 6.2 and 1.2 nm, respectively.

Figure 4 shows the Mossbauer spectra obtained for the nanocomposite with a core–shell structure. The spectra could be fitted to two sextets and a doublet. The parameters extracted by such fitting are summarized in Table II. The sextet I with $H_{int} \sim 492$ K0e is attributed to the A(tetrahedral) site of Fe_3O_4 and sextet II with $H_{int} \sim 460$ K0e is attributed to the B(octahedral) site of Fe_3O_4.[18] The central doublet is attributed to the presence of Fe^{2+} component in a silica support.[19] In our case, with the core–shell nanoparticles forming within a silica gel, both the Fe^{2+} ions at the interface of the nanoshell and the silica contribute to this Mossbauer doublet.

IV. FREQUENCY RESPONSE DATA FITTING, ANALYSES, AND CONCLUSIONS

A. Fitting models

Reference-glass and core–shell nanocomposite data sets were first analyzed by the K0 Kohlrausch frequency response model and then by the K1 one.[13–15] The K0 model is derived by direct Fourier transformation to the
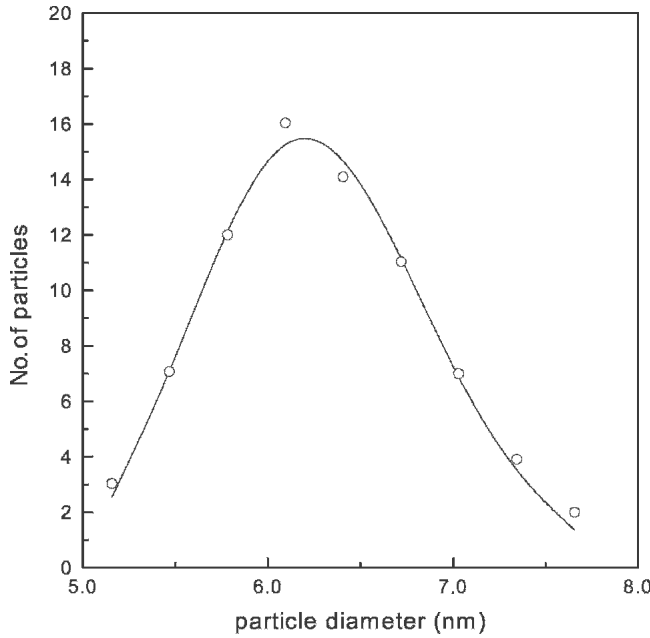
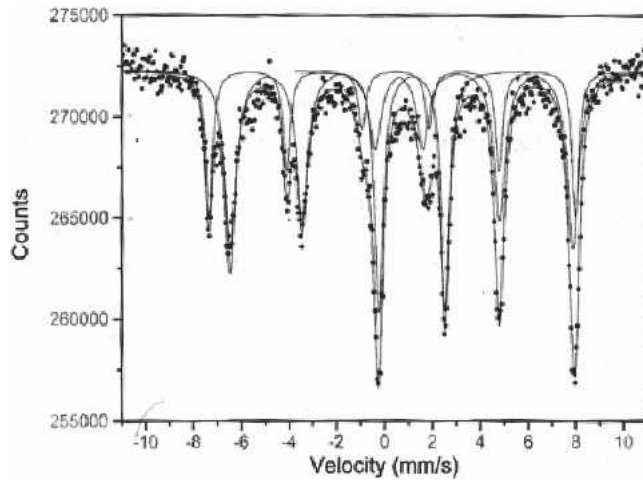FIG. 3. Histogram of composite particles shown in Fig. 2(a).

FIG. 4. Mossbauer spectra from the nanocomposite with core–shell nanostructure.

TABLE II. Mossbauer parameters extracted from Fig. 4 data.

	Isomer shift (mm/s)	Quadrupole splitting (mm/s)	Internal magnetic field (K0e)	Relative intensity (%)
Sextet I	0.36	0.05	492	23
Sextet II	0.66	0.05	460	57
Central doublet	1.17	2.86		20

quantity $I_0(\omega)$ is the normalized K0 complex resistivity response function satisfying $I_0(0) = 1$ and $I_0(\infty) = 0$. The expression for the K1-model frequency response is similar to that of Eq. (2) with $I_0(\omega)$ replaced by $I_1(\omega)$ but is indirectly, rather than directly, derived from stretched-exponential temporal response and involves a β_1 shape parameter with $0 < \beta_1 \leqslant 1$.[13–15,20,21]

The K0 and K1 models both involve the parameters ρ_{dc}, the direct current (dc) value of the complex resistivity $\rho(\omega)$; τ_0, the characteristic relaxation time of the model; and the β_0 or β_1 shape parameters. Data fitting with the K0 or K1 model requires the addition of a parallel component representing the full high-frequency limiting dielectric constant, ϵ_∞, for the K0 model and $\epsilon_{D\infty}$ for the K1 one. Here $\epsilon_{D\infty}$ is the high-frequency-limiting dielectric constant for the pure dielectric without mobile charge. In addition, fitting with the K1 model leads to an estimate of a mobile-charge effective dielectric constant $\epsilon_{C1\infty}$, so for such fitting $\epsilon_\infty = \epsilon_{C1\infty} + \epsilon_{D\infty}$. The composite models that include the parallel capacitative component are designated CK0 and CK1.

B. Fitting results

Parameter values estimated from fitting complex experimental frequency-response data sets to the CK0 and CK1 models are summarized in Table III. Because the data are noisy and of limited range, fitting results were not all found to be entirely consistent. For each temperature, the table includes estimates of the percentage relative standard deviation of the fit residuals, $100S_F$; a value of 1 is excellent. In addition, for each temperature, several different estimates of the dc resistivity ρ_{dc} are included in Table III and are discussed below.

For the reference data, the most consistent parameter estimates were obtained from CK0 fits of the $M''(\omega)$ part of the full data at the complex modulus level rather than from full complex-least-squares fitting at this level. Fits using the CK1 model (not shown) were far inferior to those presented for the CK0, but they did suggest that $\epsilon_{C1\infty}$ values were appreciably less than unity, so one expects that $\epsilon_\infty \approx \epsilon_{D\infty}$ for the CK0 results shown in Table III. Note that, as expected, both ρ_{dc} and τ_0 decrease in magnitude as the temperature increases, and the average value of β_0 is about 0.32.

frequency domain of time-domain stretched-exponential response, given by

$$\phi(t) = \exp\left[-\left(\frac{t}{\tau_0}\right)^{\beta_0}\right] \quad , \tag{1}$$

where β_0 ($0 < \beta_0 \leqslant 1$) is the stretching parameter and τ_0 is the characteristic conductivity relaxation time. For conductive systems $\phi(t)$ represents the correlation function of the mobile charge carriers. K0-model response, expressed at the complex modulus level, may be written as

$$M_{K0}(\omega) = M'_{K0}(\omega) + iM''_{K0}(\omega) \equiv i\omega\epsilon_\nu I_0(\omega) \quad , \tag{2}$$

where $M(\omega) = 1/\epsilon(\omega)$, ϵ is the complex dielectric permittivity, and ϵ_ν is the permittivity of vacuum. The

TABLE III. Parameters estimated by fitting experimental data with the CK0 and K1 CK1 models. For the reference glass, only CK0-M'' fit results are shown, and those for the nanocomposites are complex-M data-fit ones. ρ_{dc} quantities shown in parentheses are $\sigma'(\omega)$-fit estimates and those in brackets are dc measurement ones.

Specimen	Temperature (K)	Model	$100S_F$	$10^{-6}\rho_{dc}$ (ohm cm)	$\epsilon_{C1\infty}$	$\epsilon_{D\infty}$	ϵ_{∞}	τ_0 (s)	β_0 or β_1
Reference glass	417	CK0	1.12	4.28 (3.62) [3.8]	⋯	⋯	28.3	1.9×10^{-5}	0.303
	428	CK0	1.48	2.63 (2.50) [2.7]	⋯	⋯	30.4	6.4×10^{-6}	0.309
	437	CK0	0.95	2.00 (2.09) [2.2]	⋯	⋯	30.9	4.4×10^{-6}	0.343
Core-shell Nanocomposite	123	CK0	4.30	0.0737	⋯	⋯	63.1	6.7×10^{-7}	0.479
		CK1	4.13	0.0742 (0.0745) [0.0419]	24.3	30.6	54.9	2.7×10^{-8}	1/3 F
	133	CK0	2.60	0.0315	⋯	⋯	57.4	2.5×10^{-7}	0.513
		CK1	2.25	0.0316 (0.0314) [0.0319]	21.0	31.5	52.5	9.8×10^{-9}	⅓ F
	143	CK0	3.46	0.0185	⋯	⋯	56.4	1.6×10^{-7}	0.513
		CK1	3.19	0.0185 (0.0184) [0.0210]	21.8	29.6	51.4	6.0×10^{-9}	⅓ F

Results were quite different for the core–shell nanocomposite material, as presented in the bottom section of Table III. Here we show fit results for the full complex $M(\omega)$ data, using both the CK0 and the CK1 models. Although the overall fit relative standard deviations are comparable for the two situations, the CK1 ones were consistently somewhat smaller than the CK0 ones. Again, the temperature dependences of both ρ_{dc} and τ_0 were as expected, but the β_0 estimates closely approximate a value of 0.5. In contrast, CK1 fits with β_1 free to vary all led to estimates very close to ⅓ so they were fixed at ⅓ (designated as ⅓ F in the table), the semi-universal Composite Universal (CUN) model.[20,21] These fit results were thus slightly improved and made more consistent. In agreement with all previous fits using the K0 and the K1 models, the τ_0 estimates are here much smaller for the latter than for the former model.

Note that the average ϵ_∞ value of the reference glass is very close to that of the average nanocomposite core-shell $\epsilon_{D\infty}$ quantity. Thus, it appears that the likely value of the latter is about 30, and it seems virtually independent of the presence of different mobile-charge behaviors since it arises from the dipolar response of the basic material. Although this important result is what one would expect, it has not been previously verified for reference and treated materials.

Although the S_F values presented in Table III provide global estimates of the goodness of fit for the different materials and temperatures, it is useful to show how the data vary with frequency for all these conditions and include point-by-point fit estimates. Figures 5 and 6 show such results for the $M'(\omega)$ fits of Table III. Fit estimates are shown by the open circles and crosses in these figures. When the center of such a symbol falls exactly at an equivalent data point (the small solid circles), the fit is virtually perfect. As shown, such agreement is appreciably better for the reference-data results
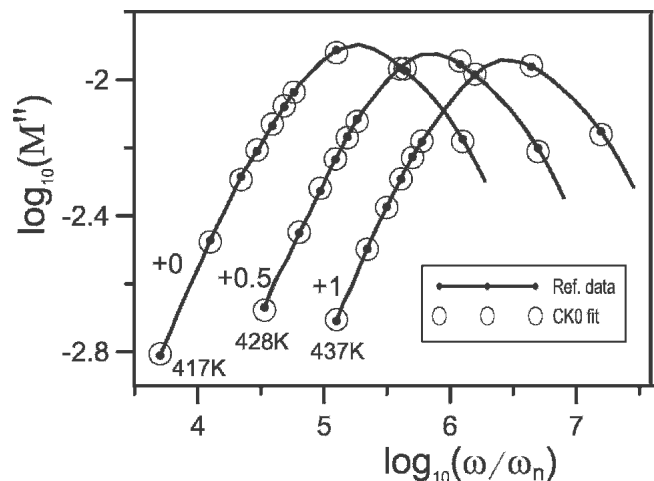

FIG. 5. Log–log plots of $M''(\omega)$ reference-glass data and $M''(\omega)$ fit points using the CK0 model with β_0 free to vary. Only every fifth data point is shown, and the 428 and 437 K curves have been shifted to the right on the $\log(\omega)$ axis by the amounts listed on the graph. Here and hereafter, ω_n is 1 rad/s.
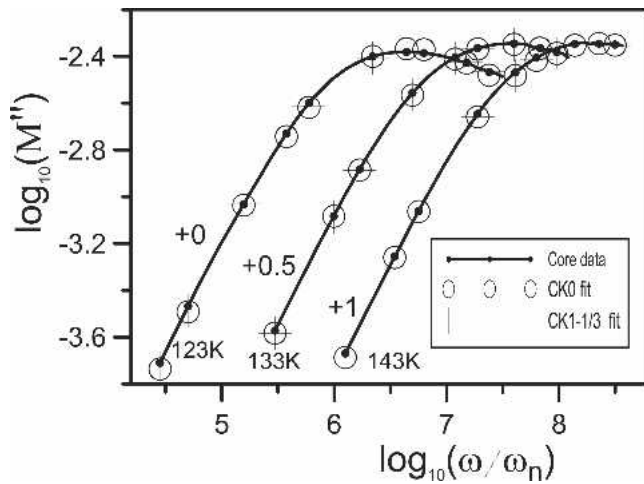
FIG. 6. Log–log plots of $M''(\omega)$ core–shell data and $M''(\omega)$ fit points following from full complex $M(\omega)$ fits, using the CK0 model with β_0 free to vary and the CK1 model with β_1 fixed at $\frac{1}{3}$. Only every seventh data point is shown, and the 428 and 437 K curves have been shifted to the right on the $\log(\omega)$ axis by the amounts listed on the graph.

FIG. 8. Log–log plots of $\sigma_{ac} \equiv \sigma'(\omega)$ core–shell data and $\sigma'(\omega)$ fit points following from fits of these real-part data sets using the CK0 model with β_0 free to vary, and from full complex $M(\omega)$ fits using the CK1 model with β_1 fixed at $\frac{1}{3}$. Only every seventh data point is shown.

of Fig. 5 than those for the core–shell data of Fig. 6. To minimize overlap and clutter, only every fifth data point is shown in Fig. 5 and every seventh one in Fig. 6, and the two higher temperature curves are shifted to the right by 0.5 and 1 units, respectively, on the log frequency axis.

Although $M(\omega)$ data sets include the effects of ϵ_∞, those involving just $\sigma'(\omega)$ do not when electrode polarization effects are negligible.[22,23] Therefore, it is important to include $\sigma'(\omega)$ data and fitting results as well as those for $M''(\omega)$. Figures 7 and 8 present such $\sigma'(\omega)$ results, where again only every fifth point is shown for the reference data and only every seventh one for the

core–shell data. The S_F values of these fits are comparable to, but somewhat larger than, those shown for the modulus fits in Table III. The data sets of Fig. 7 are appreciably more irregular than those of Fig. 8, and that for the 408 K reference data is so much so that no adequate fits were obtained.

Since the low-frequency region of the data of Fig. 7 have not reached a flat plateau approximating $\sigma_{dc} \equiv \sigma'(0)$, no good estimate of this quantity or its inverse ρ_{dc} can be obtained from the graphical behavior shown. However, estimates of ρ_{dc} are a part of CK0 and CK1 fits, and it may also be estimated from direct dc measurements. When electrode-polarization effects are present, however, dc measurements are likely to yield inaccurate estimates, as are fitting of the entire frequency response with a model that does not take account of such effects.

Table III shows for each temperature three different estimates of ρ_{dc}. The top ones for each temperature are those following from M'' fits; the ones below, in parentheses, are from CK0 and CK1-model fit estimates of ρ'; and the bottom ones, in brackets, are from direct dc measurements. Although it appears possible that a small amount of electrode-polarization effects is present, particularly for the 417 K reference-glass response, its influence seems less for the $\sigma'(\omega)$ fits than for the $M''(\omega)$ ones.

Therefore, we have used the ρ_{dc} estimates from the former fits to calculate activation energies for $T\sigma_{dc}$, the appropriate quantity following from the Nernst–Einstein equation and from the K1 model. For the reference glass, the result was 0.47 ± 0.06 eV, and for the core–shell we found 0.18 ± 0.01 eV, a much smaller value.
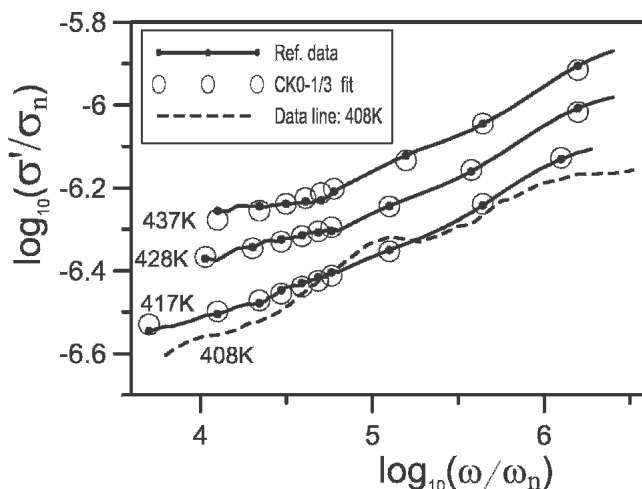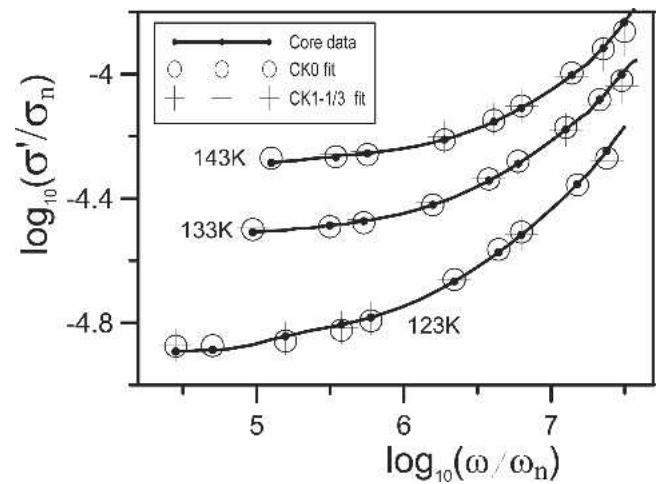

FIG. 7. Log–log plots of $\sigma_{ac} \equiv \sigma'(\omega)$ reference-glass data and $\sigma'(\omega)$ fit points following from fits of these real-part data sets, using the CK0 model with $\beta_0 = \frac{1}{3}$. Only every fifth data point is shown. Here and hereafter, $\sigma_n = 1$ mho/cm.

C. Analysis and conclusions

The average value of β_0 of about 0.32 for the reference glass suggests that the charge motion occurs along one dimension where one would expect a value of exactly $\frac{1}{3}$.[20,21] From the electron micrograph of Fig. 1, it is evident that the iron-rich phase has an interconnected configuration; the width of this phase is 5.5 nm. The conductivity in this glass was earlier ascribed to a small polaron hopping between Fe^{2+} and Fe^{3+} sites.[9] Such hopping takes place along the narrow channels of the iron-rich phase. Therefore, the $\langle \beta_0 \rangle$ value of ~0.32 is consistent with one-dimensional motion of the charge carriers.

The electron micrograph of Fig. 2(a) indicates that the iron-core particles with Fe_3O_4 shells formed along the perimeter of the iron-rich phase of the reference glass. These particles therefore form a two-dimensional structure at the interface between the iron-rich and iron-deficient phases, respectively, of the reference glass. The values of β_0 of about $\frac{1}{2}$ and of β_1 of $\frac{1}{3}$ for the core–shell-structured nanocomposite suggest, ambiguously, that charge motion may occur in this two-dimensional structure with both or only one of these two dimensions being appropriate for motion.[20] Data extending to appreciably higher frequencies would be required to confirm which type of motion is actually dominant but it is noteworthy that the K0 model reaches its final power-law slope of $\sigma'(\omega)$ much quicker than does the K1 one.[21] Thus, for the present limited-range data, it seems that the two-dimensional $\beta 0 \simeq \frac{1}{2}$ results should be taken to represent the actual situation better than the K1-fit one.

The activation energies determined from $\log \rho_{dc}/T$ versus $1/T$ plots as extracted from the alternating current (ac) resistivity analysis for the reference glass and the core–shell nanocomposite glass were 0.43 ± 0.05 eV and 0.12 ± 0.01 eV, respectively. It should be noted that the temperature ranges used for the estimation of activation energies were 300–450 K and 100–250 K for the reference and the core–shell nanostructured glass, respectively.

Electrical conduction in both these materials arises due to a small polaron hopping between Fe^{2+} and Fe^{3+} sites.[9] That electrons are the charge carriers in the present set of systems was confirmed by blocking electrode measurements in which current as a function of time was found to be invariant with silver used as electrodes. This, coupled with the fact that the values of dc resistivity as obtained from dc measurements and those obtained from ac measurements were in reasonable agreement, substantiates that only electronic transport causes the dc conduction.

The difference in the activation energy arises due to a difference in the effective dielectric constant as experienced by the hopping charge in the two materials. In the reference glass, the effective dielectric constant is ~30

whereas in nanocomposite it is ~60, as found from the CK0 and CK1 model fits discussed above. According to the Austin–Mott model,[24] the activation energy W can be written as

$$W = \frac{e^2}{4\epsilon_p r_p} \quad , \tag{3}$$

where e is magnitude of the electronic charge, ϵ_p the effective dielectric constant, and r_p is the polaron radius. Substituting the above values of ϵ_p in Eq. (3), we estimate the values of r_p equal to about 0.3 Å and 0.5 Å for the reference glass and nanocomposite glass, respectively. It is thus likely that the polaron radius increases in the interfacial amorphous phase as compared to that in the reference glass. The higher values of ϵ_p and r_p in the nanostructured glass contribute to a drastic reduction in the activation energy for polaron hopping.

In summary, ac electrical conductivity of a gel-derived iron-silicate glass was measured. Iron core–iron oxide shell nanocomposites was grown within the glass matrix, and ac electrical properties were studied. Mossbauer spectra confirmed the presence of Fe_3O_4 in the nanoshells. Electrical conductivities of both the glass systems were analyzed using both the CK0 and CK1 Kohlrausch-related frequency response fitting models and suggested the presence of interesting and potentially important differences in charge motion between the reference and treated materials.

REFERENCES

1. A. Zaslavsky, C. Aydin, S. Luryi, S. Cristoloveanu, D. Mariolle, D. Fraboulet, and S. Deleonibus: Ultrathin silicon-on-insulator vertical tunneling transistor. *Appl. Phys. Lett.* **83**, 1653 (2003).
2. L.Y. Gorelik, R.I. Shekhter, V.M. Vinokur, D.E. Feldman, V.I. Kozub, and M. Jonson: Electrical manipulation of nanomagnets. *Phys. Rev. Lett.* **91**, 088301 (2003).
3. S.I. Bozhevolnyi, S.V. Volkov, K. Leosson, and A. Boltasseva: Bend loss in surface plasmon polariton band-gap structures. *Appl. Phys. Lett.* **79**, 1076 (2001).

4. R. Krishnan, M.A. Hahn, Z. Yu, J. Silcox, P.M. Fauchet, and T.D. Krauss: Polarization surface-charge density of single semiconductor quantum rods. *Phys. Rev. Lett.* **92**, 216803 (2004).

5. V. Baltz, J. Sort, B. Rodmacq, B. Dieny, and S. Landis: Size effects on exchange bias in sub-100 nm ferromagnetic–antiferromagnetic dots deposited on prepatterned substrates. *Appl. Phys. Lett.* **84**, 4923 (2004).

6. S. Morup and C. Frandsen: Thermoinduced magnetization in nanoparticles of antiferromagnetic materials. *Phys. Rev. Lett.* **92**, 217201 (2004).

7. P. Keblinski, S.R. Phillpot, D. Wolf, and H. Gleiter: Thermodynamic criterion for the stability of amorphous intergranular films in covalent materials. *Phys. Rev. Lett.* **77**, 2965 (1996).

8. F. Huang, B. Gilbert, H. Zhang, and J.F. Banfield: Reversible, surface-controlled structure transformation in nanoparticles induced by an aggregation state. *Phys. Rev. Lett.* **92**, 155501 (2004).

9. D. Das, S. Roy, J.W. Chen, and D. Chakravorty: Interface controlled electrical and magnetic properties in Fe–Fe_3O_4–silica gel nanocomposites. *J. Appl. Phys.* **91**, 4573 (2002).

10. K.L. Ngai, J.N. Mundy, H. Jain, O. Kanert, and G. Balzer-Jollenbeck: Correlation between the activation enthalpy and Kohlrausch exponent for ionic conductivity in alkali aluminogermanate glasses. *Phys. Rev. B* **39**, 6169 (1989).

11. S.R. Elliott and F.E.G. Henn: Application of the Anderson–Stuart model to the ac conduction of ionically conducting materials. *J. Non-Cryst. Solids* **116**, 179 (1990).

12. K.J. Rao and M. Harish Bhat: Investigation of lithium chloride–lithium borate–tellurium dioxide glasses: An example of complex anionic speciation. *Phys. Chem. Glasses* **42**, 255 (2001).

13. J.R. Macdonald: Scaling and modeling in the analysis of dispersive relaxation of ionic materials. *J. Appl. Phys.* **90**, 153 (2001).

14. J.R. Macdonald: New model for nearly constant dielectric loss in conductive systems: Temperature and concentration dependencies. *J. Chem. Phys.* **116**, 3401 (2002).

15. J.R. Macdonald: Comparison and evaluation of several models for fitting the frequency response of dispersive systems. *J. Chem. Phys.* **118**, 3258 (2003).

16. J.R. Macdonald, S. Basu, and D. Chakravorty: Analysis of conducting-system frequency response data for an interfacial amorphous phase of copper-core oxide- shell nanocomposites. *J. Chem. Phys.* **122**, 214703 (2005).

17. A.K. Maity, D. Nath, and D. Chakravorty: Electrical conduction in nanocomposites of copper in silicate glasses. *J. Phys.: Condens. Matter* **8**, 5717 (1996).

18. E. Murad and J.H. Johnston: Iron oxides and hydroxides, in *Mossbauer Spectroscopy Applied to Inorganic Chemistry,* Vol. 2, edited by G.J. Long (Plenum Press, New York, 1987), p. 514.

19. S. Morup, B.S. Clausen, and H. Topsoe: Magnetic properties of microcrystals studied by Mossbauer spectroscopy. *Phys. Scr.* **25**, 713 (1982).

20. J.R. Macdonald and J.C. Phillips: Topological derivation of shape exponents for stretched exponential relaxation. *J. Chem. Phys.* **122**, 074510 (2005).

21. J.R. Macdonald: Universality, the Barton Nakajima Namikawa relation, and scaling for dispersive ionic materials. *Phys. Rev. B* **71**, 184307 (2005).

22. J.R. Macdonald: On two incompatible models for dispersion in ionic conductors. *J. Appl. Phys.* **95**, 1849 (2004).

23. J.R. Macdonald: Analysis of dispersed frequency response for ionic glasses: Influence of electrode and nearly constant loss effects. *J. Phys.: Condens. Matter* **17**, 4369 (2005).

24. I.G. Austin and N.F. Mott: Polarons in crystalline and non-crystalline materials. *Adv. Phys.* **18**, 41 (1969).